Structural Requirements of Histone Deacetylase Inhibitors: SAHA Analogs Modified on the Hydroxamic Acid

Anton V. Bieliauskas[*], **Sujith V. W. Weerasinghe**[**], **Ahmed T. Negmeldin**, **Mary Kay H. Pflum**

Department of Chemistry, Wayne State University, Detroit, MI, USA

Abstract

Histone deacetylase (HDAC) proteins have emerged as targets for anti-cancer therapeutics, with several inhibitors used in the clinic, including suberoylanilide hydroxamic acid (SAHA, vorinostat). Because SAHA and many other inhibitors target all or most of the 11 human HDAC proteins, the creation of selective inhibitors has been studied intensely. Recently, inhibitors selective for HDAC1 and HDAC2 were reported where selectivity was attributed to interactions between substituents on the metal binding moiety of the inhibitor and residues in the 14-Å internal cavity of the HDAC enzyme structure. Based on this earlier work, we synthesized and tested SAHA analogs with substituents on the hydroxamic acid metal binding moiety. The *N*-substituted SAHA analogs displayed reduced potency and solubility, but greater selectivity, compared to SAHA. Docking studies suggested that the *N*-substituent accesses the 14-Å internal cavity to impart preferential inhibition of HDAC1. These studies with *N*-substituted SAHA analogs are consistent with the strategy exploiting the 14-Åinternal cavity of HDAC proteins to create HDAC1/2 selective inhibitors.

Keywords

Docking studies; HDAC inhibitors; Histone deacetylase; Isoform selectivity; Vorinostat

Introduction

Histone deacetylase (HDAC) proteins play an important role in gene expression by governing the acetylation state of lysine residues located on the amino-terminal tails of nucleosomal histone proteins [1]. Due to their fundamental role in gene expression, HDAC proteins have been associated with basic cellular events and disease states, including cell growth, differentiation, and cancer formation [2]. As a result, HDAC proteins have emerged as attractive targets for anti-cancer therapy. Several HDAC inhibitor (HDACi) drugs are in various stages of clinical trials [3], with suberoylanilide hydroxamic acid, vorinostat (SAHA, Fig. 1) gaining FDA approval in 2006 for the treatment of advanced cutaneous T-

Correspondence: Prof. Mary Kay H. Pflum, Department of Chemistry, Wayne State University, 5101 Cass Avenue, Detroit, MI 48201, USA. .pflum@wayne.edu, **Fax:** +1-313-577-8822.

[*]Current address: Ash Stevens, Inc., 18655 Krause Street, Riverview, MI 48193, USA.

[**]Current address: Department of Molecular & Integrative Physiology, University of Michigan Medical School, 1137 E Catherine Street, Ann Arbor, MI 48109, USA.

The authors have declared no conflict of interest.

cell lymphoma (CTCL) [4]. Consistent with their clinical effects, inhibitors of HDAC proteins suppress tumor cell proliferation, induce cell differentiation, and upregulate crucial genes associated with anti-cancer effects, such as p21 [5]. Therefore, HDACi drugs represent a promising next generation of anti-cancer therapeutics.

Many HDACi drugs in and out of clinical trials, including SAHA, inhibit all HDAC isoforms nonspecifically (so called pan-inhibitors) [6]. The HDAC family contains 11 metal-dependent proteins in humans, which are separated into three classes based on their size, cellular localization, number of catalytic active sites, and homology to yeast HDAC proteins. Class I includes HDAC1–3, and 8. Class II consists of six HDAC proteins – HDAC4–7, 9, and 10. HDAC11 is the sole member of class IV, based on phylogenetic analysis [7]. It is a matter of debate whether inhibiting the entire HDAC family is required for anti-cancer activity [8]. However, elucidating the individual functions of HDAC protein family members is impossible using pan-inhibitors. Selective HDAC inhibitors that affect a single HDAC isoform (isoform-selective HDACi) would be ideal pharmacological tools to elucidate the individual functions of each HDAC isoform. In addition, isoform-selective HDAC inhibitors might provide a more effective chemotherapeutic compared to pan-inhibitors [9].

Toward creating isoform selective inhibitors, the three structural regions of the inhibitors (Fig. 1) have been modified, focusing primarily on the capping region and metal binding moiety [10]. The high sequence similarity within the active sites of the isoforms makes inhibitor design problematic [10]. Recently, the structures of HDAC1–4, 7, and 8 were reported [11–17], along with homology models of the other HDAC isoforms [18, 19]. According to structural analysis, a 14-Å internal cavity exists deep within the HDAC active site near the catalytic metal atom, which functions as an exit channel for release of the acetate byproduct after acetyl-lysine deacetylation [20–22]. Important for inhibitor development, several compounds have been designed to target the internal cavity by appending large aromatic groups to the metal binding moiety [15, 23, 24]. For example, compound **1** (Fig. 1) displays selectivity for HDAC1 and HDAC2 compared to HDAC3–8 [25, 26]. Docking studies of **1** into the HDAC1 and HDAC3 homology models suggested that selectivity was due to differential interactions of the aryl group on the metal binding group with residues in the 14-Å internal cavity [26]. A significant conclusion of these studies is that the metal binding moiety can be modified to create selective HDAC inhibitors.

To further exploit the 14-Å internal cavity for selective inhibitor design, we created SAHA analogs functionalized on the amine of the hydroxamic acid metal binding moiety. Like the benzamide of compound **1** [15], crystallographic and modeling analyses indicate that the hydroxamic acid is positioned at the base of the active site channel adjacent to the internal cavity [11–19, 27]. Given the HDAC1/2 selectivity of compound **1** [26], we hypothesized that alkyl or aryl groups attached to the hydroxamic acid of SAHA would also impart selectivity.

Results and discussion

Inhibitor synthesis

To create *N*-modified SAHA analogs, suberic acid **3** was refluxed in acetic acid to produce suberic anhydride **4** (Scheme 1), with subsequent ring opening with aniline to produce **5**. Separately, *O*-benzylhydroxylamine **6** was Boc-protected and then alkylated with various alkyl and aryl halides to produce **8**. The Boc group on *N*-Boc, *O*-benzylhydroxylamine **7** was necessary to increase the acidity of the amine proton and facilitate alkylation [28]. However, alkylation of hydroxyl amine **6** with a benzyl group proceeded directly to give the *O,N*-dibenzyl hydroxyl amine **9**, which was subsequently coupled with suberoylanilide acid **5** to produce *O*-benzyl protected analogs **10c**. For the other analogs, deprotection of **8** using TFA and neutralization was necessary prior to coupling. Finally, hydrogenolysis of **10a–e** afforded removal of the *O*-benzyl protecting group to give hydroxamic acids **2a–e**.

Inhibitor screening with lysates

HDAC inhibitory activities of analogs **2a–e** were measured using the Fluor de Lys™ *in vitro* fluorescence activity assay (Biomol Inc.) and the HDAC activity from HeLa cell lysates. All analogs showed significantly reduced potency compared to SAHA (Table 1). Pentyl variant **2b** displayed the most potent activity with a 153μM IC_{50} value, which is 1700-fold reduced compared to the parent SAHA (0.090μM, Table 1). In contrast, the methyl variant **2a** was the least potent with a 794μM IC_{50} value, which is >8800-fold reduced compared to SAHA. The benzyl analog **2c** demonstrated an intermediate IC_{50} of 293μM. Unfortunately, the homobenzyl and biphenyl variants **2d** and **2e** displayed low solubility at high concentrations, prohibiting IC_{50} determination. The percentage activity remaining at the highest concentration of analog tested (250μM) suggested that **2d** and **2e** demonstrate IC_{50} values of >500μM (Table 1). While the *N*-substituent significantly reduced the potency of the analogs, these studies with HeLa cell lysates do not assess their selectivities.

Inhibitor screening with HDAC1, 3, and 6

To assess selectivity, the analogs were screened against three individual HDAC isoforms, HDAC1, 3, and 6. HDAC1 and 3 were included because compound **1** was able to discriminate between them in prior work [25, 26]. HDAC6 was also tested to assess class II selectivity. The analogs were initially screened against the isoforms at a single concentration of 125 μM (Fig. 2). The compounds containing aliphatic substituents (**2a**, methyl; and **2b**, pentyl) displayed little to no isoform selectivity, similar to SAHA [6]. Likewise, the *N*-homobenzyl analog **2d** also showed roughly similar potency against the isoforms. In contrast, the *N*-benzyl **2c** and *N*-biphenyl **2e** variants displayed preferential HDAC1 inhibition, similar to compound **1**. Among these two analogs, *N*-biphenyl SAHA **2e** demonstrated the greatest preference, with 58±2% activity remaining with HDAC1 but statistically insignificant inhibition observed with both HDAC3 and HDAC6. The single concentration selectivity screen points to *N*-biphenyl **2e** as a preferential HDAC1 inhibitor, similar to compound **1**.

Based on the observation that the benzyl **2c** and biphenyl **2e** variants displayed HDAC1 preference at 125 μM concentration, IC_{50} values were determined (Table 2). As expected [6],

the pan-inhibitor SAHA displayed less than a 1.5-fold preference for any HDAC isoform tested [29]. The benzyl variant **2c** displayed a modest preference for HDAC1 versus HDAC3 (2.5-fold). The *N*-biphenyl variant **2e** displayed preferential inhibition for HDAC1, with an IC_{50} of $233\pm40\mu M$. Unfortunately, due to insolubility at high concentrations, IC_{50} values for HDAC3 and HDAC6 could not be determined. However, at the highest concentration possible (250 μM), no inhibitory activity was observed with either HDAC3 or HDAC6 (Supporting Information Table S11), suggesting a preference for HDAC1.

Docking studies

Docking studies were performed to rationalize the lower potency and HDAC1 preference of the *N*-modified SAHA analogs. SAHA, along with the *N*-pentyl **2b** and *N*-biphenyl **2e** analogs, were docked into the HDAC1 crystal structure [13]. SAHA displayed five interactions (1.1–3.8Å distances) with the bound Zn^{2+} metal and nearby amino acids (H140, H141, and Y303, Fig. 3A, see residues in blue). In contrast, the *N*-pentyl **2b** variant maintained only three of these interactions (with Zn^{2+}, H141, and Y303, Fig. 3B), while the *N*-biphenyl **2e** analog contained only two (with Zn^{2+} and Y303, Fig. 3C). The loss of hydrogen bonding by the hydroxamic acid amine likely accounts for the fewer stabilizing interactions with the analogs. In addition, the orientation of the hydroxamic acid is altered by the *N*-modification. Specifically, SAHA positions the carbonyl adjacent to Y303, the amine near H141, and the hydroxyl next to H140. Due to the *N*-modification, the hydroxyl amine orientation is flipped with *N*-pentyl **2b** positioning the hydroxyl near H141. Likewise, the *N*-biphenyl analog adopts an alternative pose with the carbonyl interacting with Zn^{2+} and the hydroxyl interacting with Y303. The docking experiments point toward fewer interactions between the hydroxamic acid and the active site, likely due to flipping of the *N*-modification into the 14-Å cavity and loss of hydrogen bonding, which account for the reduced potency.

In addition to the loss of bonding interactions, another significant observation from the docking studies is the positioning of the *N*-modification within the 14-Å internal cavity. The narrowest section of the cavity is created by M30, R34, and L139 (Fig. 3A and Supporting Information Fig. S9A, see resides in purple). While the pentyl group of **2b** is positioned up to this constricted point in the cavity (Fig. 3B), the biphenyl group of **2e** extends beyond the narrow opening (Fig. 3C). Therefore, the reduced potency of *N*-biphenyl SAHA **2e** may also be due to the narrowing of the cavity near M30, R34, and L139 to constrict binding (Supporting Information Fig. S9A). Consistent with the extent and orientation of interactions, the energies of the inhibitor/HDAC1 complexes for SAHA, *N*-pentyl SAHA **2b**, and *N*-biphenyl SAHA **2e** were −5.46, −4.25, and −3.28kcal/mole, respectively. The energies are consistent with the experimental data indicating that SAHA is the most potent compound, whereas the *N*-biphenyl **2e** analog is the least potent (Table 1).

The docking studies were further analyzed to explain the enhanced preference of **2e** for HDAC1 compared to SAHA and **2b** (Table 2). Prior docking analysis with compound **1** suggested that selectivity for HDAC1 compared to HDAC3 was a result of congestion in the 14-Å cavity due to a tyrosine in HDAC3; HDAC1 contains serine at the same position, which allows the cavity to accommodate bulky aromatic groups [26]. Docking of SAHA into

the HDAC3 structure revealed that Y107 is positioned relatively distant to the 14-Å cavity (Fig. 4A) [13, 14]. Likewise, S113 in the HDAC1 crystal structure is also located adjacent to the cavity (Supporting Information Fig. S10). In addition, previous mutagenesis studies indicated that S113 is only partially responsible for the potency of compound **1** with HDAC1 [21].

An alternative hypothesis explaining the HDAC1 preferences of compound **1** and *N*-biphenyl SAHA **2e** emerges when considering the narrowest point in the 14-Å internal cavities of HDAC1 and HDAC3. HDAC3 maintains a considerably more constricted 14-Å internal cavity than HDAC1 (compare Fig. 4A to Fig. 3A). The residues M24, R28, and L133 of HDAC3 appear to block the cavity and may restrict access to bulky *N*-modified inhibitors. Docking of *N*-biphenyl **2e** into the HDAC3 crystal structure produced no poses that were consistent with the expected metal/hydroxamic binding interaction. Instead, the biphenyl group was positioned up to the narrowest section of the cavity, near M24, R28, and L133 of HDAC3 (Fig. 4C and Supporting Information Fig. S9B). In this case, the biphenyl group is unable to extend beyond the constricted region to access the 14-Å internal cavity of HDAC3, as was seen with HDAC1 (Fig. 3C and Supporting Information Fig. S9A). As a result of the blocked cavity, the hydroxamic acid is positioned at the outside edge of the active site channel, unable to interact with the metal ion. Therefore, docking suggests that the poor potency observed with **2e** and HDAC3 is due to restricted access of the *N*-biphenyl to the 14-Å internal cavity, which prevents favorable metal/hydroxamic acid interactions. In contrast, the straight chain *N*-pentyl analog **2b** is positioned up to the constriction point (Fig. 4B), similar to HDAC1 (Fig. 3B), which allows effective binding and better potency. In total, the docking studies are consistent with accessibility of the 14-Å cavity to large aromatic groups as a significant factor leading to the HDAC1 preference of inhibitors bearing substituents on the metal binding group, including compound **1** and *N*-biphenyl SAHA **2e**.

Discussion

N-modified SAHA analogs (**2a**–**e**) displayed significantly reduced potency compared to the parent SAHA. Interestingly, the benzyl and pentyl substituents are tolerated to a greater extent than any of the other *N*-substituted analogs. Docking studies are consistent with the pentyl groups accessing the 14-Å internal cavities of HDAC1 and HDAC3 (Figs. 3B and 4B). However, the additional interactions in the cavity were unable to overcome the lost hydrogen bonding due to the presence of the *N*-modification. The results suggest that any group, regardless of size, incorporated directly on the hydroxamic acid will result in decreased inhibitory activity compared to the unsubstituted analog. These studies are consistent with prior work reporting reduced potencies of HDAC inhibitors as a result of *N*-methylation of the hydroxamic acid group [30, 31].

Although the *N*-modified SAHA analogs showed reduced potency compared to SAHA, one compound displayed HDAC1 preference. The *N*-biphenyl variant **2e** showed an IC$_{50}$ of 233 μM with HDAC1, while not inhibiting HDAC3 or 6 at the highest concentration allowed (250 μM). Docking analysis with the HDAC1 and HDAC3 crystal structures suggests that that accessibility to the 14-Å internal cavity is differentially restricted, leading to preferential binding to HDAC1 over HDAC3. Therefore, the combined experimental and computational

analyses of *N*-modified SAHA analogs further validate the concept of creating isoform-selective HDAC inhibitors by positioning aromatic substituents in the 14-Å internal cavity. These studies guide future inhibitor design by suggesting that additional substituted metal binding groups can be created to take advantage of the altered cavity accessibility of the HDAC isoforms.

Experimental

Chemistry

General methods—Unless otherwise noted, all manipulations were carried out under inert argon atmosphere in flame-dried glassware. "Iron-free" glassware was prepared by soaking in a 6M HCl acid bath overnight. Tetrahydrofuran (THF) was freshly distilled before use from sodium benzophenone ketyl, dichloromethane (CH_2Cl_2) was freshly distilled before use from CaH_2, and triethylamine was freshly distilled before use from CaH_2. Flash chromatography was carried out using 60-Å, 230–400 mesh silica gel. All organic reagents were used as purchased from Acros Organics, Fisher Scientific, or Sigma–Aldrich. NMR spectra were taken on either a Varian Unity 300 MHz, Varian L900 400 MHz, or a Varian 500 MHz. IR spectra were taken on a Jasco FT/IR – 4100. HRMS data were obtained on either a Waters LCT Premier XE ESI-LC–MS TOF or a Waters GCT EI-TOF. Syringe filters used were 0.22 μm Millipore Millex Syringe Drive Filter Unit, PES express.

Please also see the Supporting Information for the InChI codes and selected biological activities of the compounds **2a**–**e**.

Preparation of suberic anhydride (4)—Suberic anhydride (**4**) was synthesized as described [32]. Accordingly, suberic acid (5.0 g, 28.8 mmol) was added to acetic anhydride (10 mL) and refluxed for 1 h. The mixture was then evaporated to remove excess acetic anhydride. The residue was recrystallized several times from acetonitrile to give suberic anhydride (2.0 g, 45%). All spectra were identical with those described in the literature.

Preparation of 8-oxo-8-(phenylamino)octanoic acid (5)—8-Oxo-8-(phenylamino)octanoic acid (**5**) was synthesized as described [32]. Suberic anhydride (1.0 g, 6.4 mmol) was dissolved in THF (10 mL). Aniline (0.6 mL, 6.4 mmol) was then added and the solution was allowed to stir for 30 min. The mixture was diluted with water (100 mL) and the formed solid was filtered and recrystallized from water to give 8-oxo-8-(phenylamino)octanoic acid (1.6 g, 55%). All spectra were identical with those described in the literature.

Preparation of tert-butyl benzyloxycarbamate (7)—*tert*-Butyl benzyloxycarbamate was synthesized as described [33]. Accordingly, to a flask containing *O*-benzylhydroxylamine hydrochloride (1.0 g, 6.23 mmol) was added dioxane (7 mL). Di-*tert*-butyl dicarbonate (1.33 mL, 6.23 mmol) was added, followed by a 1M solution of $NaHCO_3$ (6.23 mL, 6.23 mmol). Vigorous evolution of gas was observed. The solution was allowed to stir overnight. The mixture was then evaporated to remove dioxane. To the residue was added a 1M solution of citric acid (until pH was ~4). The mixture was then extracted with

dichloromethane (3×25 mL). The organic layers were pooled, dried over magnesium sulfate, filtered, and evaporated to afford *tert*-butyl benzyloxycarbamate (1.4 g, 99%). All spectra were identical with those described in the literature.

Typical procedure for the generation of tert-butyl benzyloxy(alkyl)carbamate (8)—*tert*-Butyl benzyloxy(alkyl)carbamate was synthesized as described [33]. Accordingly, to a flask containing 1 equiv. of *tert*-butyl benzyloxycarbamate (**7**) was added THF (to make a 0.1M solution) followed by 1.25 equiv. of sodium hydride (60% dispersion on mineral oil). Vigorous evolution of gas was observed as the flask was allowed to stir for 30 min. The alkyl halide (1.25 equiv.) was then added and the mixture was heated overnight. The mixture was filtered through celite, evaporated to an oil, and purified using flash silica gel chromatography (5% ethyl acetate/hexanes) to afford *tert*-butyl benzyloxy(alkyl)carbamate as a clear oil.

Preparation of tert-butyl benzyloxy(methyl)carbamate (8a)—Methyl iodide (0.0704 mL, 1.13 mmol) gave **8a** (0.2105 g, 98%) ^{1}H NMR (500 MHz, CDCl$_3$): δ 1.50 (s, 9H), 3.05 (s, 3H), 4.85 (s, 2H), 7.30–7.40 (m, 5H); ^{13}C NMR (125 MHz, CDCl$_3$): δ 28.5, 37.0, 77.0, 81.0, 128.5, 129.5, 136.0, 157.0.

Preparation of tert-butyl benzyloxy(pentyl)carbamate (8b)—Bromopentane (0.28 mL, 2.2 mmol) gave **8b** (0.1095 g, 23%). ^{1}H NMR (500 MHz, CDCl$_3$): δ 0.90 (t, 3H), 1.30 (m, 4H), 1.50 (s, 9H), 1.65 (t, 2H), 3.40 (t, 2H), 4.85 (s, 2H), 7.35–7.41 (m, 5H); ^{13}C NMR (125 MHz, CDCl$_3$): δ 14.2, 22.2, 27.0, 28.5, 29.2, 50.0, 77.0, 81.5, 128.5, 129.5, 136.0, 157.0; IR: 2958, 2932, 2871, 1702, 1455, 1367, 1276, 1150, 747, 699cm^{-1}. HRMS (ESI-LC–MS, *m/z*); found: [M+Na], 316.1896, calcd. for C$_{27}$H$_{27}$NO$_3$Na, 316.1889.

Preparation of tert-butyl benzyloxy(phenethyl)carbamate (8d)—(2-Bromoethyl)benzene (0.19 mL, 1.35 mmol) gave **8d** (0.2367 g, 80%). ^{1}H NMR (500 MHz, CDCl$_3$): δ 1.43 (s, 9H), 2.90 (t, 2H), 3.60 (t, 2H), 4.80 (s, 2H), 7.20–7.50 (m, 10H); ^{13}C NMR (125 MHz, CDCl$_3$): δ 28.4, 33.5, 41.8, 77.0, 81.8, 126.5, 129.0, 129.4, 129.5, 130.0, 136.0, 139.0, 157.0; IR: 2976, 2932, 1699, 1366, 1157, 746, 698cm^{-1}.

Preparation of tert-butyl benzyloxy(biphenyl-4-ylmethyl)-carbamate (8e)—4-(Bromomethyl)biphenyl (0.2793 g, 1.13 mmol) gave **8e** (0.3268 g, 93%). ^{1}H NMR (500 MHz, CDCl$_3$): δ 1.50 (s, 9H), 4.61 (s, 2H), 4.7 (s, 2H), 7.32 (m, 6H), 7.45 (m, 4H), 7.60 (dd, 4H); ^{13}CNMR(125 MHz, CDCl$_3$): δ 29.0, 54.0, 77.0, 82.0, 127.5, 127.7, 129.0, 129.2, 129.4, 129.8, 135.8, 136.1, 141.0, 141.2, 157.0; IR: 2975, 2930, 1698, 1366, 1159, 1082, 757, 697cm^{-1}; HRMS (ESI-LC–MS, *m/z*); found: [M+Na], 412.1886, calcd. for C$_{25}$H$_{27}$NO$_3$Na, 412.1889.

Typical procedure for the generation of N^1-(benzyloxy)-N^1-alkyl-N^8-phenyloctanediamide (10)—To a flask containing 1.5 equiv. of *tert*-butyl benzyloxy(alkyl)carbamate (**8**) was added a 50% TFA in dichloromethane solution (0.16M solution based on **8**) and the mixture was allowed to stir for 10 min (until completeness visualized by TLC, Rf=0 compared with Rf=0.5 for **8**, 5% ethyl acetate in hexanes). The mixture was then evaporated to remove TFA. The residue was dissolved in dichloromethane

and washed with sat. NaHCO$_3$ (1×volume to organic layer) to neutralize the remaining TFA. The aqueous layer was then washed with dichloromethane (2×volume to aqueous layer). The organic layers were pooled, dried over magnesium sulfate, filtered, and evaporated to give the deprotected amine. To the flask containing the amine was then added acetonitrile (0.1M solution based on acid **5**), 1 equiv. of 8-oxo-8-(phenylamino)-octanoic acid (**5**), 1.5 equiv. of TBTU, and 1.25 equiv. of diisopropylethylamine, successively. The mixture was allowed to stir overnight. The reaction was then quenched with 1M HCl aqueous solution and extracted with ethyl acetate (3×volume to aqueous layer). The organic layers were pooled, dried over magnesium sulfate, filtered, and evaporated to an oil. Flash silica gel chromatography (5% methanol, 45% dichloromethane, 50% hexanes) afforded N^1-(benzyloxy)-N^1-alkyl-N^8-phenyloctanediamide (**10**) as a clear oil.

Preparation of N^1-(benzyloxy)-N^1-methyl-N^8-phenyloctanediamide (10a)—*tert*-Butyl benzyloxy(methyl)carbamate (**8a**) (0.20 g, 0.84 mmol) gave **10a** (0.1469 g, 71%). ^{1}H NMR (500 MHz, CDCl$_3$): δ 1.30 (m, 4H), 1.60 (m, 2H), 1.70 (m, 2H), 2.30–2.38 (m, 4H), 3.20 (s, 3H), 4.8 (s, 2H), 7.1 (t, 1H), 7.3 (m, 2H), 7.40 (m, 5H), 7.55 (d, 2H), 7.85 (bs, 1H); ^{13}C NMR (125 MHz, CDCl$_3$): δ 24.5, 25.5, 29.0, 29.2, 32.5, 34.0, 37.5, 76.5, 120.0, 124.0, 129–129.8 (m), 135.0, 139.0, 171.5, 176.0; IR: 3309, 2930, 2857, 1660, 1599, 1541, 1498, 1440, 1176, 977, 753, 698 cm^{-1}; HRMS (ESI-LC–MS, *m/z*); found: [M], 368.2099, calcd. for C$_{22}$H$_{28}$N$_2$O$_3$, 368.2100.

Preparation of N^1-(benzyloxy)-N^1-pentyl-N^8-phenyloctanediamide (10b)—*tert*-Butyl benzyloxy(pentyl)carbamate (**8b**) (0.1 g, 0.34 mmol) gave **10b** (0.1217 g, 84%). ^{1}H NMR (500 MHz, CDCl$_3$): δ 0.90 (t, 3H), 1.25–1.40 (m, 8H), 1.60 (m, 4H), 1.72 (t, 2H), 2.35 (t, 2H), 2.40 (m, 2H), 3.65 (m, 2H), 4.80 (s, 2H), 7.1 (t, 1H), 7.3 (t, 2H), 7.40 (m, 5H), 7.60 (d, 2H), 7.9 (bs, 1H); ^{13}C NMR (125 MHz, CDCl$_3$): δ 14.0, 22.5, 24.8, 25.5, 27.0, 29.0, 29.1, 29.2, 32.4, 37.8, 45.8, 77.0, 120.0, 124.0, 129.0–129.4 (m), 135.0, 138.5, 171.0, 175.0; IR: 3308, 2931, 2858, 1661, 1599, 1541, 1498, 1440, 753, 697cm^{-1}. HRMS (ESI-LC–MS, *m/z*); found: [MþH], 425.2799, calcd. for C$_{26}$H$_{37}$N$_2$O$_3$, 425.2804, found: [M+Na], 447.2611, calcd. for C$_{26}$H$_{36}$N$_2$O$_3$, 447.2624.

Preparation of N^1-(benzyloxy)-N^1-phenethyl-N^8-phenyloctanediamide (10d)—*tert*-Butyl benzyloxy(phenethyl)carbamate (**8d**) (0.2367 g, 0.72 mmol) gave **10d** (0.1422 g, 65%). ^{1}H NMR (500 MHz, CDCl$_3$): δ 1.30 (m, 2H), 1.35 (m, 2H), 1.58 (m, 2H), 1.70 (m, 2H), 2.30–2.40 (m, 4H), 2.91 (t, 2H), 3.90 (m, 2H), 4.80 (s, 2H), 7.10 (t, 1H), 7.20 (m, 4H), 7.30 (m, 4H), 7.40 (m, 4H), 7.55 (d, 2H), 7.80 (bs, 1H); ^{13}C NMR (125 MHz, CDCl$_3$): δ 24.5, 25.5, 29.0, 29.1, 32.5, 33.5, 37.8, 47.8, 77.0, 120.0, 124.0, 127.0, 129 (m), 135.0, 138.8, 139.0, 172.0, 175.0; IR: 3311, 2931, 1660, 1599, 1540, 1497, 1440, 751, 698cm^{-1}; HRMS (ESI-LC–MS, *m/z*); found: [M], 459.2648, calcd. for C$_{29}$H$_{35}$N$_2$O$_3$, 459.2648, found: [M+Na], 481.2458, calcd. for C$_{29}$H$_{35}$N$_2$O$_3$Na, 481.2458.

Preparation of N^1-(benzyloxy)-N^1-(biphenyl-4-ylmethyl)-N^8-phenyloctanediamide (10e)—*tert*-Butyl benzyloxy(biphenyl-4-ylmethyl)carbamate (**8e**) (0.32 g, 0.82 mmol) gave **10e** (0.1724 g, 40%). ^{1}H NMR (500 MHz, CDCl$_3$): δ 1.30 (m, 4H), 1.65 (m, 2H), 1.70 (m, 2H), 2.30 (t, 2H), 2.45 (t, 2H), 4.80 (s, 2H), 4.85 (s, 2H), 7.10 (t,

1H), 7.30–7.45 (m, 12H), 7.5–7.60 (m, 6H); ^{13}C NMR (125 MHz, CDCl$_3$): δ 24.5, 25.5, 29.0, 29.1, 32.8, 37.8, 50.0, 77.0, 120.0, 124.0, 127.2, 127.4, 129.0 (m), 135.0, 136.0, 138.5, 140.8, 141.0, 171.8; IR: 3308, 2930, 1660, 1599, 1541, 1498, 1488, 1440, 910, 755, 698cm^{-1}; HRMS (ESI-LC–MS, *m/z*); found: [M+Na], 543.2628, calcd. for C$_{34}$H$_{36}$N$_2$O$_3$Na, 543.2624.

Preparation of N, O-dibenzylhydroxylamine (9)—*N, O*-Dibenzylhydroxylamine was synthesized as described previously [34]. Accordingly, *O*-benzylhydroxylamine (2 g, 9.4 mmol) hydrochloride was dissolved in DMF (50 mL). Potassium carbonate (5.2 g, 37.5 mmol) was added to the flask followed by benzyl bromide (1.5 mL, 12.5 mmol). The mixture was stirred overnight. The reaction was quenched with water (30 mL) and extracted with CH$_2$Cl$_2$ (4 × 20 mL). The organic layers were pooled and evaporated to an oil. To remove residual DMF, the oil was dissolved in 20mL of diethyl ether and extracted with water (3 × 20 mL). The ethereal layer was dried over magnesium sulfate, filtered, and evaporated to an oil. Flash silica gel chromatography (5% ethyl acetate in hexanes) afforded 1.83 g of a clear oil (67%). All spectra were identical with those described in the literature.

Preparation of N^1-benzyl-N^1-(benzyloxy)-N^8-phenyloctanediamide (10c)—To a flask containing *N,O*-dibenzylhydroxylamine (**9**) (0.1920 g, 0.9 mmol) was added acetonitrile (6 mL), 8-oxo-8-(phenylamino)octanoic acid (**5**) (0.15 g, 0.6 mmol), TBTU (0.28 g, 0.9 mmol), and diisopropylethylamine (0.21 mL, 1.2 mmol), successively. The general procedure was followed to produce **10**, except that the chromatography solvent was 30–40% ethyl acetate/hexanes, which afforded *N*^{1}-benzyl-*N*^{8}-(benzyloxy)-N^8-phenyloctanediamide (**10c**) (0.1754 g, 63%).^{1}H NMR (500 MHz, CDCl$_3$): δ 1.30 (m, 4H), 1.60 (m, 2H), 1.70 (m, 2H), 2.30 (t, 2H), 2.42 (t, 2H), 4.75 (s, 2H), 4.81 (s, 2H), 7.10 (t, 1H), 7.25–7.38 (m, 12H), 7.55 (d, 2H), 7.60 (bs, 1H); ^{13}C NMR (125 MHz, CDCl$_3$): δ 24.2, 25.8, 29.0, 29.1, 32.3, 37.8, 50.5, 77.0, 120.0, 124.0, 128.0, 128.72, 128.8, 128.9, 129.15, 129.42, 135.0, 137.0, 138.5, 171.8; IR: 3315, 2932, 1661, 1599, 1541, 1497, 1440, 1308, 911, 753, 698cm^{-1}; HRMS (EI-TOF, *m/z*); found: [M], 444.2424, calcd. for C$_{28}$H$_{32}$N$_2$O$_3$, 444.2413.

Typical procedure for the generation of N^1-hydroxy-N^1-alkyl-N^8-phenyloctanediamide (2)—To an acid washed flask containing 1 equiv. of *N*^{1}-(benzyloxy)-*N*^{1}-alkyl-N^8-phenyloctanediamide (**10**) was added ethyl acetate (0.1 M solution) and 0.1 equiv. of 10% palladium on carbon. The flask was vacuum purged several times with argon and then hydrogen before incubation under hydrogen for 2 h with stirring (until completeness visualized by TLC, Rf=0 compared with Rf=0.5 for **9**, 30% ethyl acetate in hexanes). The mixture was filtered and then solvents evaporated to afforded *N*^{1}-hydroxy-*N*^{1}-alkyl-N^8-phenyloctanediamide (**2**) as a white solid.

Preparation of N^1-hydroxy-N^1-methyl-N^8-phenyloctanediamide (2a)—*N*^{1}-(Benzyloxy)-*N*^{1}-methyl-N^8-phenyloctanediamide (**10a**) (0.1400 g, 0.39 mmol) gave **2a** (0.1070 g, 98%). ^{1}H NMR (500 MHz, CD$_3$OD): δ 1.40 (m, 4H), 1.60 (m, 2H), 1.70 (m, 2H), 2.35 (t, 2H), 2.45 (t, 2H), 3.19 (s, 3H), 7.10 (t, 1H), 7.30 (t, 2H), 7.50 (d, 2H); ^{13}C NMR (125 MHz, CD$_3$OD): δ 25.0, 25.8, 29.0, 29.1, 31.9, 35.0, 36.8, 120.0, 124.0, 128.5, 139.0,

173.5, 175.0; HRMS (EI-TOF, *m/z*); found: [M], 278.1635, calcd. for $C_{15}H_{22}N_2O_3$, 278.1630.

Preparation of N[1]-pentyl-N[1]-hydroxy-N[8]-phenyloctanediamide (2b)—*N[1]*-(Benzyloxy)-*N[1]*-pentyl-*N[8]*-phenyloctanediamide (**10b**) (0.12 g, 0.28 mmol) gave **2b** (0.0860 g, 88%). ^{1}H NMR (500 MHz, CD3OD): δ 0.90 (t, 3H), 1.25–1.43 (m, 8H), 1.63 (m, 4H), 1.70 (m, 2H), 2.39 (t, 2H), 2.49 (t, 2H), 3.60 (t, 2H), 7.10 (t, 1H), 7.30 (t, 2H), 7.55 (d, 2H); ^{13}C NMR (125 MHz, CD3OD): δ 13.0, 22.2, 24.8, 25.8, 26.1, 28.78, 28.9, 29.0, 32.0, 36.9, 47.8, 120.0, 124.0, 128.8, 138.9, 173.5, 174.8; IR: 3310, 3190, 2930, 1663, 1617, 1600, 1573, 1549, 1510, 1500, 1465, 1258, 1214, 1173, 1033, 751, 725, 690 cm^{-1}; HRMS (ESI-LC–MS, *m/z*); found: [M+H], 335.2345, calcd. for $C_{19}H_{31}N_2O_3$, 335.2335, found: [M+Na], 357.2151, calcd. for $C_{19}H_{31}N_2O_3Na$, 357.2154.

Preparation of N[1]-benzyl-N[1]-hydroxy-N[8]-phenyloctanediamide (2c)—*N[1]*-Benzyl-*N[1]*-(benzyloxy)-*N[8]*-phenyloctanediamide (**10c**) (0.17 g, 0.38 mmol) gave **2c** (0.1223 g, 91%). ^{1}H NMR (500MHz, CD3OD): δ 1.40 (m, 4H), 1.65 (m, 4H), 2.35 (t, 2H), 2.50 (t, 2H), 4.85 (s, 2H), 7.10 (t, 1H), 7.30 (m, 7H), 7.55 (d, 2H);^{13}C NMR (125MHz, CD3OD) 0.0, 124.0, 127.5, 128.1, 128.2, 128.5, 137.0, 139.0, 173.5, 175.0; IR: 3304, 3136, 2937, 1660, 1596, 1531, 1497, 1468, 1443, 1204, 1181, 754, 720, 696 cm^{-1}; HRMS (EI-TOF, *m/z*); found: [M], 354.1957, calcd. for $C_{21}H_{26}N_2O_3$, 354.1943.

Preparation of N[1]-hydroxy-N[1]-phenethyl-N[8]-phenyloctanediamide (2d)—*N[1]*-(Benzyloxy)-*N[1]*-phenethyl-*N[8]*-phenyloctanediamide (**10d**) (0.14 g, 0.31 mmol) gave **2d** (0.0791 g, 69%). ^{1}H NMR (500 MHz, CD3OD): δ 1.31–1.40 (m, 4H), 1.55 (m, 2H), 1.70 (m, 2H), 2.35 (t, 2H), 2.45 (t, 2H), 2.90 (t, 2H), 3.80 (t, 2H), 7.10 (t, 1H), 7.15–7.30 (m, 7H), 7.55 (d, 2H); ^{13}C NMR (125 MHz, CD3OD): δ 24.5, 25.5, 28.8, 29.0, 32.0, 32.8, 36.7, 49.0, 120.0, 124.0, 126.0, 128.2, 128.3, 128.5, 139.0, 174.0, 175.0; IR: 3167, 2932, 2849, 1649, 1600, 1499, 1463, 1413, 1191, 753, 691 cm^{-1}. HRMS (ESI-LC–MS, *m/z*); found: [M+H], 369.2195, calcd. for $C_{22}H_{29}N_2O_3$, 369.2178, found: [M+Na], 391.2015, calcd. for $C_{22}H_{28}N_2O_3Na$, 391.1998.

Preparation of N[1]-(biphenyl-4-methyl)-N[1]-hydroxy-N[8]-phenyloctanediamide (2e)—*N[1]*-(Benzyloxy)-*N[1]*-(biphenyl-4-ylmethyl)-*N[8]*-phenyloctanediamide (**10e**) (0.1700 g, 0.33 mmol) gave **2e** (0.0986 g, 69%).^{1}H NMR (500 MHz, DMSO): δ 1.30 (m, 4H), 1.55 (m, 4H), 2.25 (t, 2H), 2.40 (t, 2H), 4.70 (s, 2H), 7.00 (t, 1H), 7.22 (m, 3H), 7.30 (m, 2H), 7.42 (t, 2H), 7.60 (m, 6H), 9.85 (bs, 1H); ^{13}C NMR (125 MHz, DMSO): δ 25.0, 25.8, 29.0, 29.1, 32.3, 37.0, 51.5, 120.0, 123.5, 127.0, 128.0, 129.0, 129.1, 129.3, 137.0, 139.8, 140.0, 140.5, 172.0, 174.0; HRMS (ESI-LC–MS, *m/z*); found: [M+H], 431.2342, calcd. for $C_{27}H_{31}N_2O_3$, 431.2335, found: [M+Na], 453.2159, calcd. for $C_{27}H_{30}N_2O_3Na$, 453.2154.

HDAC activity assay

HDAC activity was measured using the Fluor de Lys™ assay (Biomol), as previously reported [35, 36]. To measure global HDAC inhibition, 0.5 μL of HeLa lysates (~4 μg of total protein) diluted up to 24 μL with HDAC assay buffer (50 mM Tris, pH 8.0, 137 mM NaCl, 2.7 mM KCl, 1 mM MgCl2) was incubated without (1 μL of DMSO) or with small

molecule inhibitor (1 μL of $50 \times$ stock solution in DMSO, final concentrations of inhibitors indicated in Fig. 2 and Supporting Information Tables S1–S11) for 30min at 30°C with shaking. To perform the isoform selective studies, HDAC1 (0.2 μg, specific activity=42.5 pmol/min/μg), HDAC3 (0.05μg, specific activity=249 pmol/min/μg) or HDAC6 (0.25μg, specific activity=257 pmol/min/μg) purchased from BPS Biosciences was used. After the preincubation period, Fluor de Lys™ substrate (25 μL) in HDAC assay buffer was added (to give a final concentration of 100 μM for HeLa lysate, 50 μM for HDAC1, or 25 μM for HDAC3 and 6 in a total reaction volume of 50 μL). The reaction mixture was incubated at 30°C for 45 min with shaking. Fluor de Lys™ developer (2.5 μL of 20× stock solution diluted up to 50 μL in HDAC assay buffer) was added (to give a 100 μL total volume) and incubated with shaking for 5 min at room temperature. The fluorescence intensity was determined (excitation at 360 nm and emission at 465 nm) using a Geniosplus Fluorimeter (Tecan). For each trial, a reaction without HDAC activity was used to assess the background. The background fluorescence without HDAC activity was subtracted from the signal observed with enzyme. Percentage deacetylase activity was calculated by dividing the background corrected fluorescence units of small molecule-treated reactions with that of untreated reactions (set at 100%) and multiplying by 100. At least three independent trials were performed with the mean and standard error reported. IC_{50} values were obtained by plotting the percentage deacetylase activity versus small molecule concentration and fitting the data to a sigmoidal dose–response curve ($y=100/(1+(x/IC_{50})^{n})$) using KaleidaGraph software (Supporting Information Figs S1–S8). Data with SAHA (lysates and isoforms) were previously reported, but included here for comparison [29].

Docking studies

Crystal structures for HDAC1 and HDAC3 were downloaded from the RCSB protein data bank (HDAC1: 4BKX and HDAC3: 4A69).PyMOL (Schrodinger, LLC) was used to delete the MTA1 corepressor chain, acetate, potassium, and sulfate ions in the HDAC1 crystal structure. In the case of the HDAC3 crystal structure, the water molecules, chain A, deacetylase-activation-domain (DAD) (from the SMRT corepressor), glycerol, D-myo-inositol-1,4,5,6-tetrakisphosphate molecules, acetate, potassium, and sulfate ions were deleted. AutoDockTools-1.5.4 program [37, 38] was used to add all hydrogen atoms, modify histidine protonation (H140 and H141 residues for HDAC1, His134 and His135 for HDAC3) by adding only HD1, compute Gasteiger charges, and merge all nonpolar hydrogen, followed by generation of the pdbqt output file. The charge of the zinc atom was manually changed from zero to +2. A grid box with a spacing of 0.375Å, size of $56 \times 42 \times 38$, and coordinates for the center of the grid box (−48.000, 18.000, −3.750) were used for HDAC1, while the values for HDAC3 were $58 \times 58 \times 54$ and (8.166, 76.663, 21.318). The map type was set by choosing the ligand and then AutoGrid 4.2 was used to pre-calculate and generate the grid maps files required for the docking calculations. All the docked compounds were drawn in ChemBioDraw Ultra and Chem 3D Pro was used to run MM2 job for energy minimization. Then AutoDockTools-1.5.4 program was used to add hydrogens, compute Gasteiger charges, merge nonpolar hydrogens, choose torsions, and generate the pdbqt files. All acyclic bonds were made rotatable except amide bonds. AutoDock 4.2 program [38] was used to perform the docking calculations using a genetic algorithm. The generated pdbqt file for the enzyme was set as a rigid macromolecule and the genetic algorithm search

parameters were set to 100 GA runs for each ligand with a population size of 150, a maximum number of 2.5×10^5 energy evaluations, a maximum number of 2.7×10^4 generations, a mutation rate of 0.2, and a crossover rate of 0.8. The docking parameters were set to default. All the output DLG files were converted to pdbqt format and the results were visualized in PyMOL. The lowest energy pose consistent with metal binding is discussed in the text.

Supplementary Material

Refer to Web version on PubMed Central for supplementary material.

Acknowledgments

References

[1]. Wu J, Grunstein M, Trends Biochem. Sci 2000, 25, 619–623. [PubMed: 11116189]

[2]. Minucci S, Pelicci PG, Nat. Rev. Cancer 2006, 6, 38–51. [PubMed: 16397526]

[3]. Garber K, Nat. Biotech 2007, 25, 17–19.

[4]. Grant S, Easley C, Kirkpatrick P, Nat. Rev. Drug Discov 2007, 6, 21–22. [PubMed: 17269160]

[5]. Mai A, Massa S, Rotili D, Cerbara I, Valente S, Pezzi R, Simeoni S, Ragno R, Med. Res. Rev 2005, 25, 261–309. [PubMed: 15717297]

[6]. Khan N, Jeffers M, Kumar S, Hackett C, Boldog F, Khramtsov N, Qian X, Mills E, Berghs SC, Carey N, Finn PW, Collins LS, Tumber A, Ritchie JW, Jensen PB, Lichenstein HS, Sehested M, Biochem. J 2008, 409, 581–589. [PubMed: 17868033]

[7]. Gregoretti I, Lee Y-M, Goodson HV, J. Mol. Biol 2004, 338, 17–31. [PubMed: 15050820]

[8]. Karagiannis TC, El-Osta A, Leukemia 2007, 21, 61–65. [PubMed: 17109024]

[9]. Balasubramanian S, Verner E, Buggy JJ, Cancer Lett. 2009, 280, 211–221. [PubMed: 19289255]

[10]. Bieliauskas AV, Pflum MKH, Chem. Soc. Rev 2008, 37, 1402–1413. [PubMed: 18568166]

[11]. Somoza JR, Skene RJ, Katz BA, Mol C, Ho JD, Jennings AJ, Luong C, Arvai A, Buggy JJ, Chi E, Tang J, Sang B-C, Verner E, Wynands R, Leahy EM, Dougan DR, Snell G, Navre M, Knuth MW, Swanson RV, McRee DE, Tari LW, Structure 2004, 12, 1324–1334.

[12]. Vannini A, Volpari C, Filocamo G, Casavola EC, Brunetti M, Renzoni D, Chakravarty P, Paolini C, Francesco RD, Gallinari P, Steinkuhler C, Marco SD, Proc. Natl. Acad. Sci. U S A 2004, 101, 15064–15069. [PubMed: 15477595]

[13]. Millard CJ, Watson PJ, Celardo I, Gordiyenko Y, Cowley SM, Robinson CV, Fairall L, Schwabe JWR, Mol. Cell 2013, 51, 57–67. [PubMed: 23791785]

[14]. Watson PJ, Fairall L, Santos GM, Schwabe JW, Nature 2012, 481, 335–340. [PubMed: 22230954]

[15]. Bressi JC, Jennings AJ, Skene R, Wu Y, Melkus R, Jong RD, O'Connell S, Grimshaw CE, Navre M, Gangloff AR, Bioorg. Med. Chem. Lett 2010, 20, 3142–3145. [PubMed: 20392638]

[16]. Bottomley MJ, Lo Surdo P, Di Giovine P, Cirillo A, Scarpelli R, Ferrigno F, Jones P, Neddermann P, De Francesco R, Steinkuhler C, Gallinari P, Carfi A, J. Biol. Chem 2008, 283, 26694–26704. [PubMed: 18614528]

[17]. Schuetz A, Min J, Allali-Hassani A, Schapira M, Shuen M, Loppnau P, Mazitschek R, Kwiatkowski NP, Lewis TA, Maglathin RL, McLean TH, Bochkarev A, Plotnikov AN, Vedadi M, Arrowsmith CH, J. Biol. Chem 2008, 283, 11355–11363. [PubMed: 18285338]

[18]. Estiu G, Greenberg E, Harrison CB, Kwiatkowski NP, Mazitschek R, Bradner JE, Wiest O, J. Med. Chem 2008, 51, 2898–2906. [PubMed: 18412327]

[19]. Wang DF, Helquist P, Wiech NL, Wiest O, J. Med. Chem 2005, 48, 6936–6947. [PubMed: 16250652]

[20]. Wang DF, Wiest O, Helquist P, Lan-Hargest HY, Wiech NL, J. Med. Chem 2004, 47, 3409–3417. [PubMed: 15189037]

[21]. Wambua MK, Nalawansha DA, Negmeldin AT, Pflum MK, J. Med. Chem 2014, 57, 642–650. [PubMed: 24405391]

[22]. Haider S, Joseph CG, Neidle S, Fierke CA, Fuchter MJ, Bioorg. Med. Chem. Lett 2011, 21, 2129–2132. [PubMed: 21320778]

[23]. Moradei OM, Mallais TC, Frechette S, Paquin I, Tessier PE, Leit SM, Fournel M, Bonfils C, Trachy-Bourget MC, Liu JH, Yan TP, Lu AH, Rahil J, Wang J, Lefebvre S, Li ZM, Vaisburg AF, Besterinan JM, J. Med. Chem 2007, 50, 5543–5546. [PubMed: 17941625]

[24]. Di Micco S, Chini MG, Terracciano S, Bruno I, Riccio R, Bifulco G, Bioorg. Med. Chem 2013, 21, 3795–3807. [PubMed: 23693069]

[25]. Witter DJ, Harrington P, Wilson KJ, Chenard M, Fleming JC, Haines B, Kral AM, Secrist JP, Miller TA, Bioorg. Med. Chem. Lett 2008, 18, 726–731. [PubMed: 18060775]

[26]. Methot JL, Chakravarty PK, Chenard M, Close J, Cruz JC, Dahlberg WK, Fleming J, Hamblett CL, Hamill JE, Harrington P, Harsch A, Heidebrecht R, Hughes B, Jung J, Kenific CM, Kral AM, Meinke PT, Middleton RE, Ozerova N, Sloman DL, Stanton MG, Szewczak AA, Tyagarajan S, Witter DJ, Paul Secrist J, Miller TA, Bioorg. Med. Chem. Lett 2008, 18, 973–978. [PubMed: 18182289]

[27]. Finnin MS, Donigian JR, Cohen A, Richon VM, Rifkind RA, Marks PA, Pavletich NP, Nature 1999, 401, 188–193. [PubMed: 10490031]

[28]. Sulsky R, Demers JP, Tetrahedron Lett. 1989, 30, 31–34.

[29]. Choi SE, Weerasinghe SV, Pflum MK, Bioorg. Med. Chem. Lett 2011, 21, 6139–6142. [PubMed: 21889343]

[30]. Giannini G, Marzi M, Marzo MD, Battistuzzi G, Pezzi R, Brunetti T, Cabri W, Vesci L, Pisano C, Bioorg. Med. Chem. Lett 2009, 19, 2840–2843. [PubMed: 19359173]

[31]. Lamblin M, Dabbas B, Spingarn R, Mendoza-Sanchez R, Wang TT, An BS, Huang DC, Kremer R, White JH, Gleason JL, Bioorg. Med. Chem 2010, 18, 4119–4137. [PubMed: 20452225]

[32]. Mai A, Esposito M, Sbardella G, Massa S, Org. Prep. Proced. Int 2001, 33, 391–394.

[33]. Sulsky R, Demers JP, Tetrahedron Lett. 1989, 30, 31–34.

[34]. Nicolaou KC, Mathison CJN, Montagnon T, J. Am. Chem. Soc 2004, 126, 5192–5201. [PubMed: 15099102]

[35]. Bieliauskas A, Weerasinghe S, Pflum MH, Bioorg. Med. Chem. Lett 2007, 17, 2216–2219. [PubMed: 17307359]

[36]. Choi SE, Pflum MKH, Bioorg. Med. Chem. Lett 2012, 22, 7084–7086. [PubMed: 23089527]

[37]. Sanner MF, J. Mol. Graph Model 1999, 17, 57–61. [PubMed: 10660911]

[38]. Morris GM, Huey R, Lindstrom W, Sanner MF, Belew RK, Goodsell DS, Olson AJ, J. Comput. Chem 2009, 30, 2785–2791. [PubMed: 19399780]
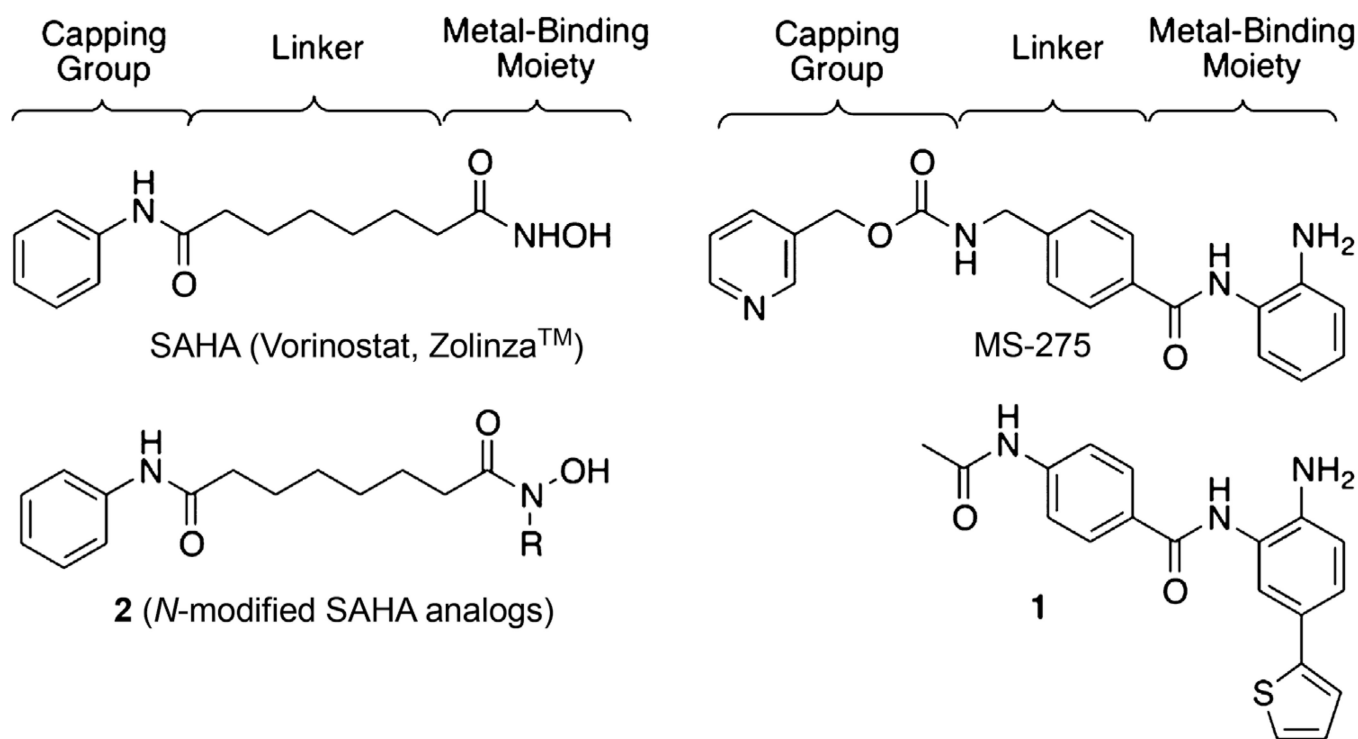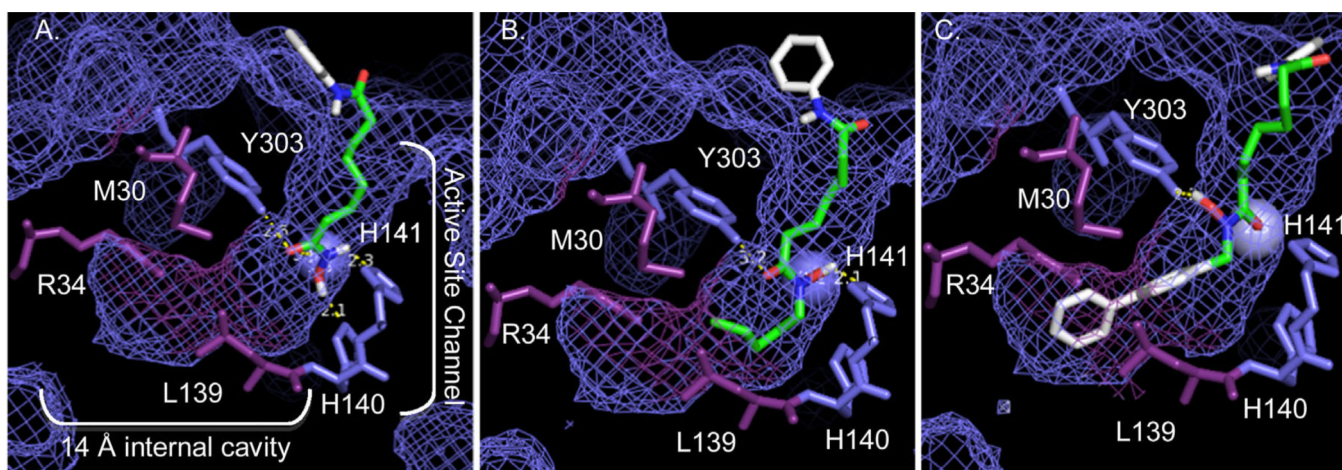
Figure 1.
Structures of select HDAC inhibitors with the structural regions indicated at the top.
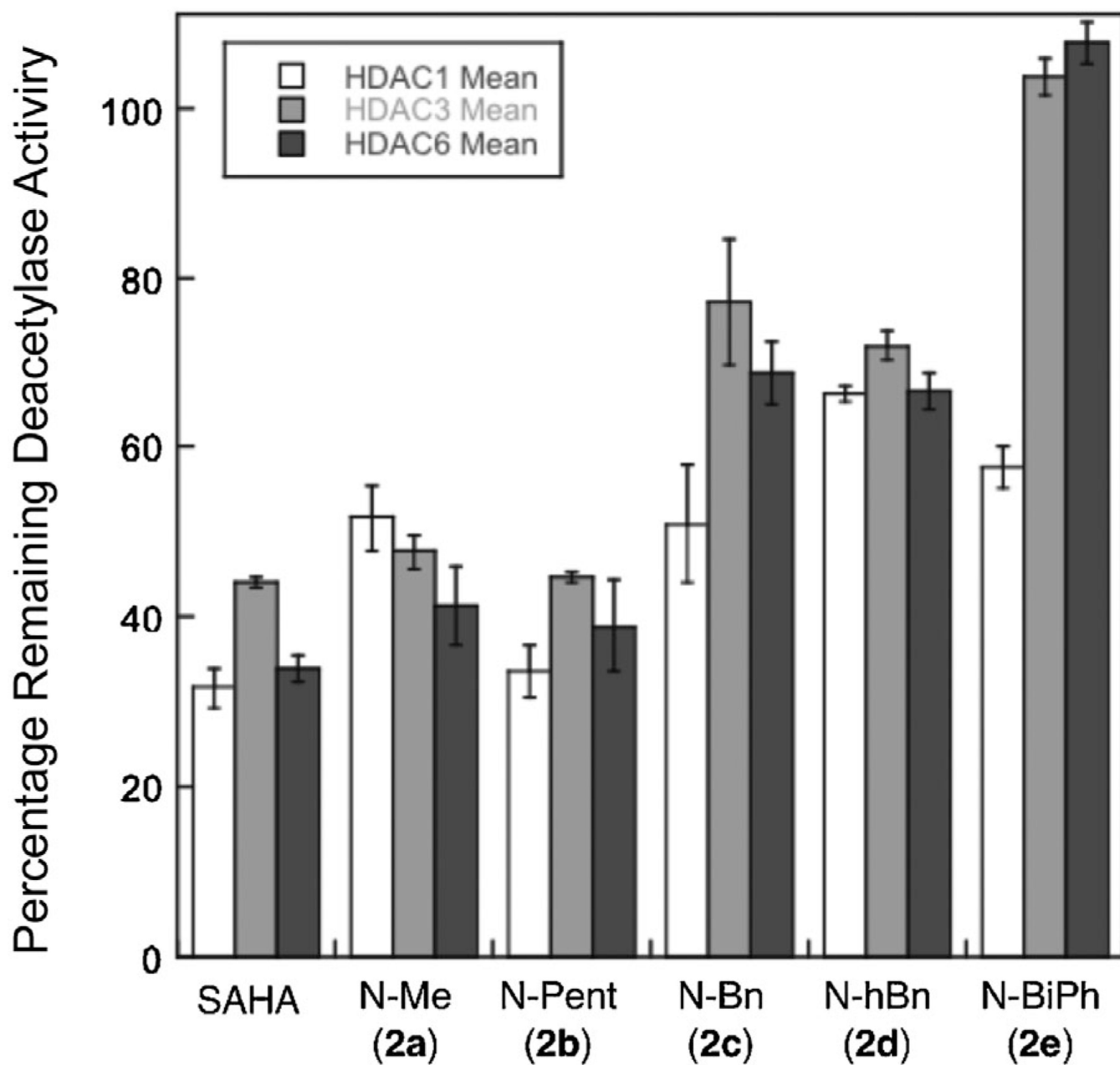
Figure 2.
HDAC inhibitory activities of the *N*-modified SAHA analogs were measured at 125 μM against HDAC1, 3, and 6. SAHA was tested at 125nM concentration. Mean percentage deacetylase activity remaining of three to five independent trials with standard error is shown (Supporting Information Table S6).

Figure 3.
Docking of SAHA (A), *N*-pentyl SAHA **2b** (B), and *N*-biphenyl SAHA **2e** (C) into the HDAC1 crystal structure (PBD 4BKX). The HDAC structure is represented as blue mesh, the Zn^{2+} metal as a blue orb, and the inhibitor and amino acids as ball and sticks. The atoms of the inhibitor are color-coded (C=green/white; O=red; N=blue, H=white).
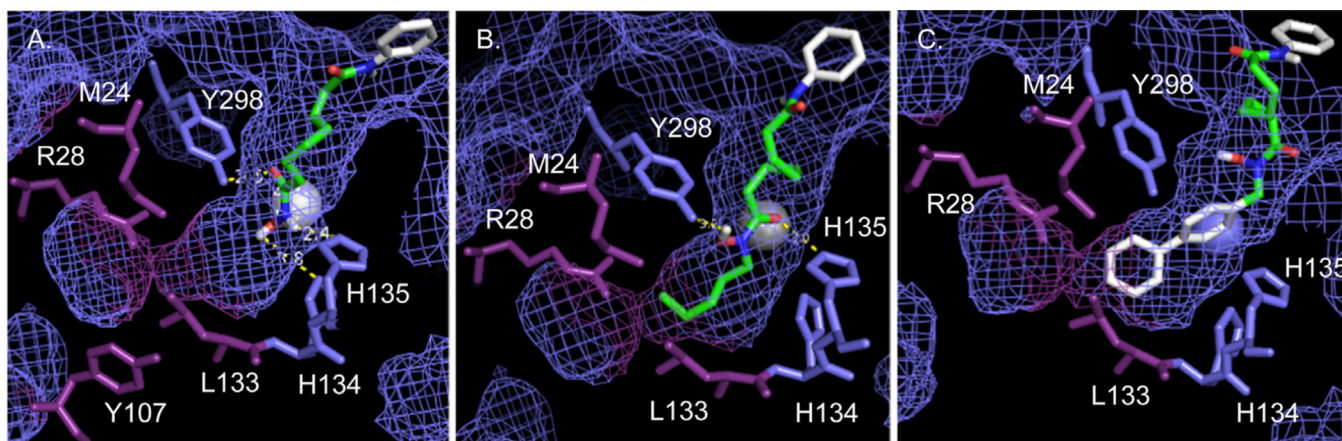
Figure 4.
Docking of SAHA (A), *N*-pentyl SAHA **2b** (B), and *N*-biphenyl SAHA **2e** (C) into the
HDAC3 crystal structure (PBD 4A69). The HDAC structure is represented as blue mesh, the
Zn^{2+} metal as a gray orb, and the inhibitor and amino acids as ball and sticks. See Fig. 3 for
color coding.
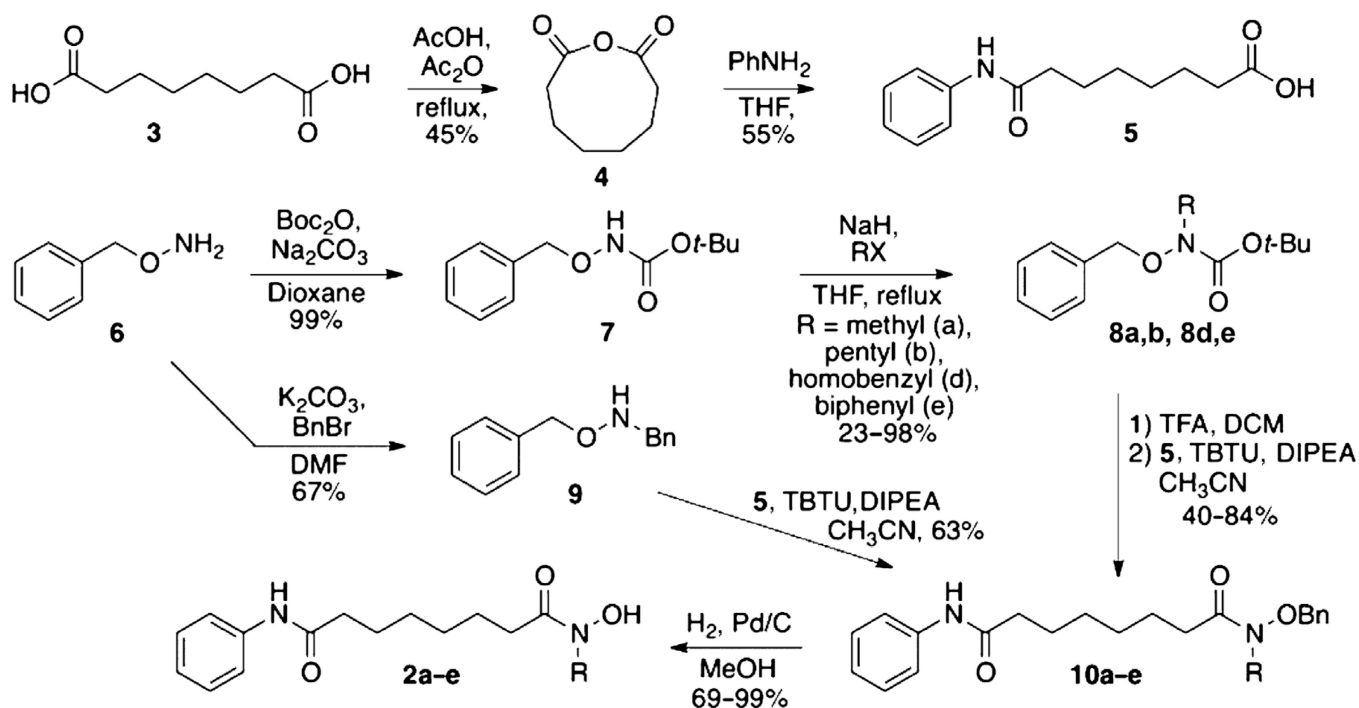
Scheme 1.
Synthesis of *N*-substituted SAHA analogs (**2a–e**).

Table 1.

HDAC inhibitory potency of 2a–e and SAHA against HeLa cell lysates.

Compounds	R	IC_{50} (μM) or % activity remaining[a]
SAHA	H	0.090 ± 0.004
2a	Methyl	794 ± 41
2b	Pentyl	153 ± 14
2c	Benzyl	293 ± 32
2d	Homobenzyl	$80 \pm 2\%$ activity at 250 μM[b]
2e	Biphenyl	$101 \pm 1\%$ activity with 250 μM[b]

[a]Values are the mean of three independent trials with standard error (Supporting Information Tables S1–S4 and Figs. S1–S4).

[b]Solubility problems prevented testing at concentrations above 250 μM. Note that assays with the methyl variant **2a** at 250 μM showed $72 \pm 5\%$ remaining activity (Supporting Information Table S5).

Table 2.

IC$_{50}$ values for SAHA, N-benzyl 2c, and N-biphenyl 2e against HDAC1, 3, and 6. [a]

	HDAC1	HDAC3	HDAC6
SAHA	0.096 ± 0.016 μM	0.146 ± 0.012 μM	0.074 ± 0.009 μM
2c	177 ± 21 μM	440 ± 23 μM	287 ± 9 μM
2e	233 ± 40 μM	$105 \pm 2\%$ [b]	$108 \pm 3\%$ [b]

[a] Values are the means of at least three independent trials with standard error (Supporting Information Tables S7–S10 and Figs. S5–S8).

[b] Deacetylase activity remaining at 250 μM concentration of inhibitor is shown (Supporting Information Table S11) because solubility issues prevented IC$_{50}$ value determination.